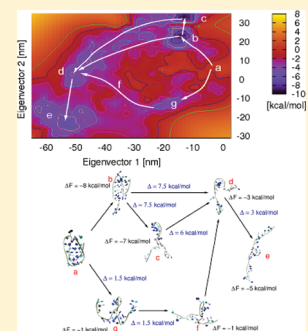


# Stable Conformations of a Single Stranded Deprotonated DNA i-Motif

Jens Smiatek,<sup>\*†</sup> Chun Chen,<sup>‡</sup> Dongsheng Liu,<sup>‡</sup> and Andreas Heuer<sup>\*†</sup><sup>†</sup>Institut für Physikalische Chemie, Universität Münster, D-48149 Münster, Germany<sup>‡</sup>Department of Chemistry, Tsinghua University, Beijing 100190, People's Republic of China

**ABSTRACT:** We present molecular dynamics simulations of a single stranded deprotonated DNA i-motif in explicit solvent. Our results indicate that hairpin structures are stable equilibrium conformations at 300 K. The entropic preference of these configurations is explained by strong water ordering effects due to the present number of hydrogen bonds. We observe a full unfolding at higher temperatures in good agreement with experimental results.



## 1. INTRODUCTION

The appearance of non-Watson–Crick-like structures in DNA was reported two decades ago.<sup>1</sup> Since that time much effort has been spent to investigate these conformations and possible applications in detail.<sup>2–5</sup> Experiments led to the conclusion that these structures are the only known DNA configurations that involve systematic base intercalation.<sup>2</sup> Prominent representatives are the G-quadruplex structures and the i-motif,<sup>5</sup> where the first one is formed by guanine (G) rich sequences<sup>3</sup> while the latter is present in more cytosine (C) rich strands of DNA.<sup>2</sup>

The stabilizing mechanism for these at first glance fragile structures is realized by a proton mediated cytosine binding between different strands or regions of the sequence resulting in a stable C–CH<sup>+</sup> pairing in acidic solution.<sup>1,2,4,5</sup> Hence it becomes clear that hemiprotonated structures are occurring at slightly acidic to neutral conditions resulting in pH values from 4.8 to 7.0.<sup>1,2,6</sup> i-Motifs show a remarkable stability<sup>6</sup> and have been found as tetrameric and dimeric complexes although their existence has also been proven for single stranded DNA.<sup>2</sup> A sketch of a single stranded i-motif with its sequence as it is used in the present study is shown in Figure 1.

Due to its biological appearance in centromeric and telomeric DNA, the distinct i-motif conformations have been discussed as a new class of possible biological targets for cancers and other diseases.<sup>7,8</sup> However, a detailed investigation of the function in the human cell is still missing. Despite this lack of knowledge, the application of this configuration in modern biotechnology has experienced an enormous growth.<sup>4</sup> Since the i-motif becomes unstable at basic pH values, a systematic decrease and increase of protons in the solution by changing the pH value results in a reversible folding and unfolding mechanism. It has been shown that this process occurs on a time scale of seconds.<sup>4,6</sup>

Technological applications for this mechanism are given by molecular nanomachines,<sup>4,9</sup> switchable nanocontainers,<sup>10</sup>

pH sensors inside living cells,<sup>11</sup> building materials for logic gate devices,<sup>12</sup> and sensors for distinguishing single walled and multi-walled carbon nanotube systems.<sup>13</sup> In addition to the experimental results, computational studies have also investigated the i-motif and validated the remarkable stability of hemiprotonated cytosine pairs.<sup>14–16</sup>

In contrast to an acidic solution, it has been reported that the deprotonated i-motif at basic or neutral pH values unfolds into unexpected hairpin conformations.<sup>17,18</sup> For a full understanding of the unfolding and folding properties, it is therefore of prior importance to study the stability of the i-motif configuration and further occurring structures also in their deprotonated forms. This is in particular true for the investigation of a grafted i-motif layer.<sup>19</sup>

In this paper we present the results of molecular dynamics simulations concerning the deprotonated single stranded DNA i-motif in dilute solution. Our main aim is focused on the thermodynamic characterization of stable conformations. We are able to observe hairpin structures as the global equilibrium conformations at 300 K via free energy calculations. The thermodynamic properties of each stable and metastable structure are studied separately. At higher temperatures our simulations indicate a transition into a fully unfolded strand. We are able to explain this effect in terms of entropic variations due to the present number of hydrogen bonds. Our numerical findings are in good agreement with experimental circular dichroism (CD) spectropolarimetry data.

The paper is organized as follows. In sections 2 and 3 we present the numerical and experimental details. The results are presented in section 4. We conclude with a brief summary in section 5.

**Received:** September 7, 2011

**Revised:** October 5, 2011

**Published:** October 13, 2011

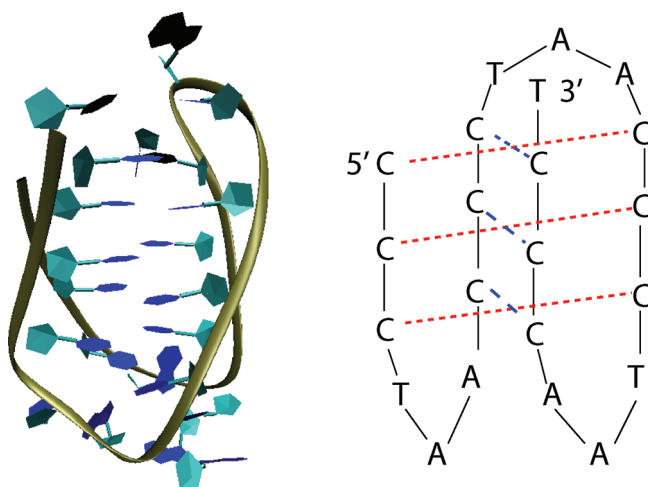


**Figure 1.** Structure of the DNA i-motif (left) with its corresponding sequence (right).

## 2. NUMERICAL DETAILS

We have performed our molecular dynamics simulations of the i-motif in explicit TIP3P solvent at 300 K by the GROMACS software package<sup>20</sup> with the implementation of the ffAMBER03 force.<sup>21–24</sup> The single DNA strand consists of 22 nucleic acids given by the sequence 5'-CCC-[TAA-CCC]<sub>3</sub>-T-3' where T, A, and C denote thymine, adenine, and cytosine. We modeled this structure which is directly related to the sequence used in ref 9 by using the PDB entry 1ELN<sup>25</sup> where uracil has been changed to thymine.

The cubic simulation box with periodic boundary conditions had dimensions of 5.41 × 5.41 × 5.41 nm and was filled with 5495 TIP3P water molecules. The negative charge of  $-22e$  of the backbone has been compensated by 22 sodium ions. We applied a Nosé–Hoover thermostat to keep the temperature constant. All bonds have been constrained by the LINCS algorithm. Electrostatics have been calculated by the PME method, and the time step was 2 fs. After energy minimization by a steepest descend method, the initial warm-up phase of 1 ns has been performed by keeping the position of the DNA restrained.

The calculation of the free energy landscape has been performed by the metadynamics method presented in ref 26. The biased metadynamics simulations at 300 K have been conducted by the program plug-in PLUMED.<sup>27</sup> The Gaussian hills were set each 2 ps with a height of 0.25 kJ/mol and a width of 0.25 nm. The corresponding reaction coordinates for the biased energy are the distance between nucleobase C1 and T22 and the distance between the center of mass for C1 and T22 to A11. The final free energy landscapes have been refined by histogram reweighting<sup>28</sup> of 15 biased simulations of 10 ns at 300 K by the method introduced in ref 29. The eigenvector free energy landscape has been calculated by the application of a projection scheme.<sup>29</sup>

Five 10 ns simulations at 500 K have been combined to calculate an unbiased high temperature averaged eigenvector set in terms of the essential dynamics concept.<sup>30</sup> Eigenvectors have been shown as useful to capture the main concerted motion of the molecule.<sup>30</sup> Mathematically the analysis of essential dynamics is closely related to principal component calculations.<sup>30</sup> The main motion is described by the first eigenvectors which form the essential subspace, whereas the fluctuating motion of the higher eigenvectors is incorporated in the remaining subspace. A detailed description can be found in refs 29 and 30.

The unbiased high temperature averaged eigenvector set was used for the projection of the free energy landscape onto the essential subspace of the first eigenvectors<sup>29,30</sup> in the low temperature regime at 300 K. In a recent publication<sup>31</sup> we have validated this method by indicating the agreement between unfolding pathways at 500 K compared to 300 K simulations. The calculation of the thermodynamic properties has been performed by keeping the position of each structure restrained for 100 ps.

## 3. EXPERIMENTAL DETAILS

The oligodeoxynucleotide was purchased from Sangon Co., Ltd. The DNA sequence was identical to the one that was used in the simulations, and it was dissolved in a final buffer with 50 mM MES and 50 mM NaCl. The buffer had a pH value of 8.0, and the concentration of DNA was 10  $\mu$ M. We used circular dichroism (CD) spectropolarimetry to investigate the structural behavior. All CD measurements were recorded on a Jasco spectropolarimeter (J-810) equipped with a programmable temperature-control unit. The range of scanning wavelength was from 350 to 220 nm for two different temperatures, 298.15 and 368.15 K.

## 4. RESULTS AND DISCUSSION

**4.1. Stable and Metastable Conformations.** The starting point for our simulations was the maximum unstable structure as presented in Figure 1. For the study of the stable conformations, we have analyzed the energetic minima and the corresponding structures by the free energy differences to the starting conformation. This can be achieved by a study of the free energy landscape which has been computed by the metadynamics method.<sup>26,32</sup> The usage of metadynamics allows to overcome energetic barriers by the application of a history dependent biasing potential. Recently it has been shown that this technique can be also used to analyze unfolding pathways.<sup>31,33,34</sup>

Along the simulation trajectories at 300 K we have observed several stable structures after the vanishing of the energetically unfavorable starting conformation. The corresponding distance matrices for the nucleobases of the initial structure and three further deprotonated conformations are presented in Figure 2. It is obvious that the deprotonated i-motif (Figure 2a) represents a well-defined structure with many local interactions even for long distances along the backbone. Two further structures (Figure 2b,c) differ in their nearest neighbor interactions. The configuration of Figure 2b is a semiopened hairpin structure with relaxed 3' end, and the conformation of Figure 2c is given by a planar hairpin conformation with crosslike interactions. Small distances for all nucleobases between C1 and A12 can be observed in Figure 2b, whereas Figure 2c indicates interactions between the opposite sides of the strand. In addition, we have also observed a fully unfolded configuration (Figure 2d) at late biased simulation times. This conformation is characterized by the absence of the crosslike structure as shown in Figure 2c. It can be concluded that only local nearest neighbor interactions along the backbone are present and base-pair stacking is nearly absent.

**4.2. Free Energy Landscapes.** The free energy landscape at 300 K for the biased collective variables as explained in section 2 is shown in Figure 3. Two large minima can be identified in a funnel-like landscape<sup>35</sup> with energy differences from the starting structure around  $-8$  kcal/mol. This result indicates them as very stable in contrast to the i-motif. Detailed examination of these

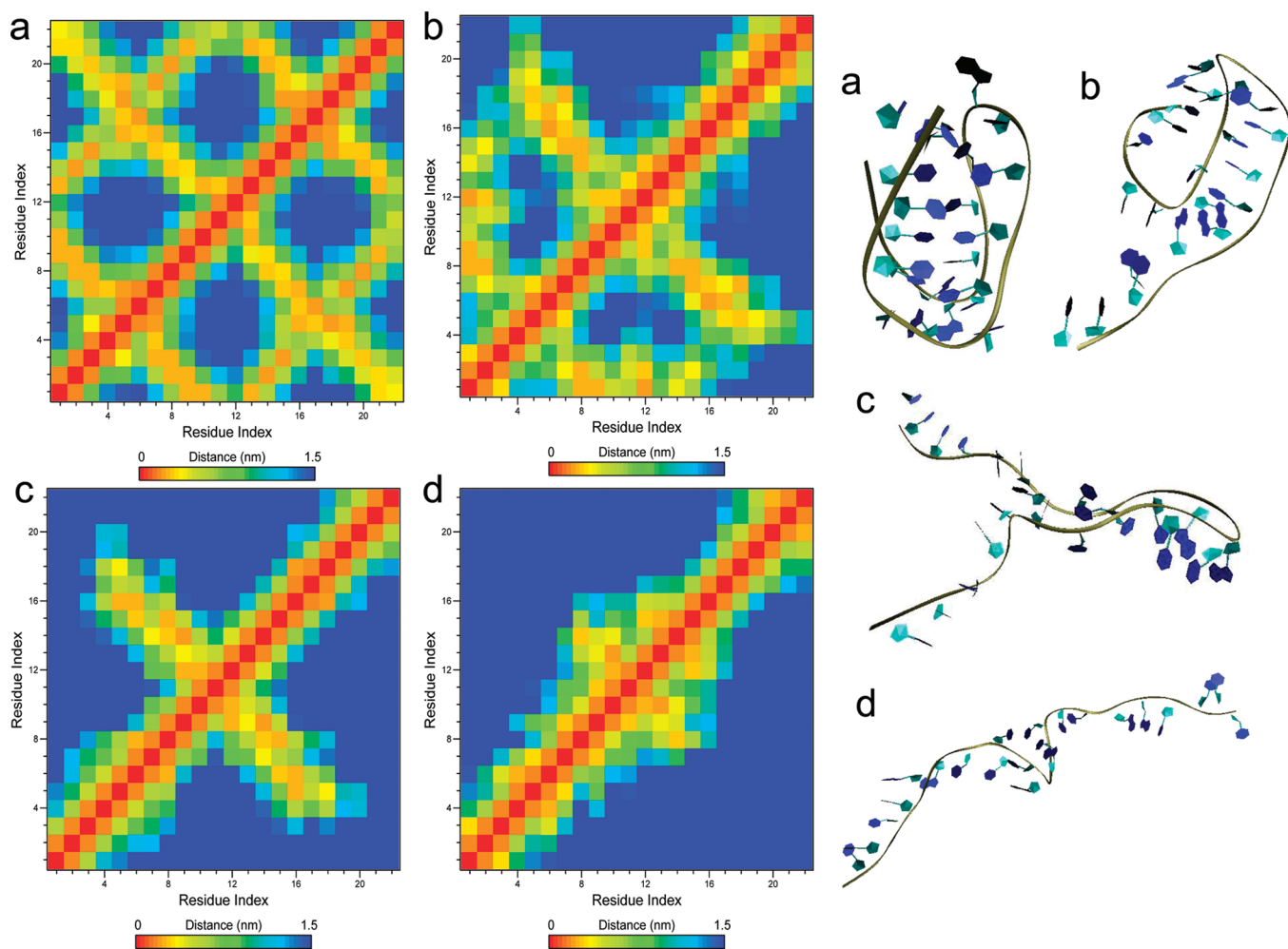


**Figure 2.** Distance matrices for different conformations. Panel a shows the initial i-motif. Panels b and c are hairpin structures, and panel d presents the results for a fully unfolded strand.

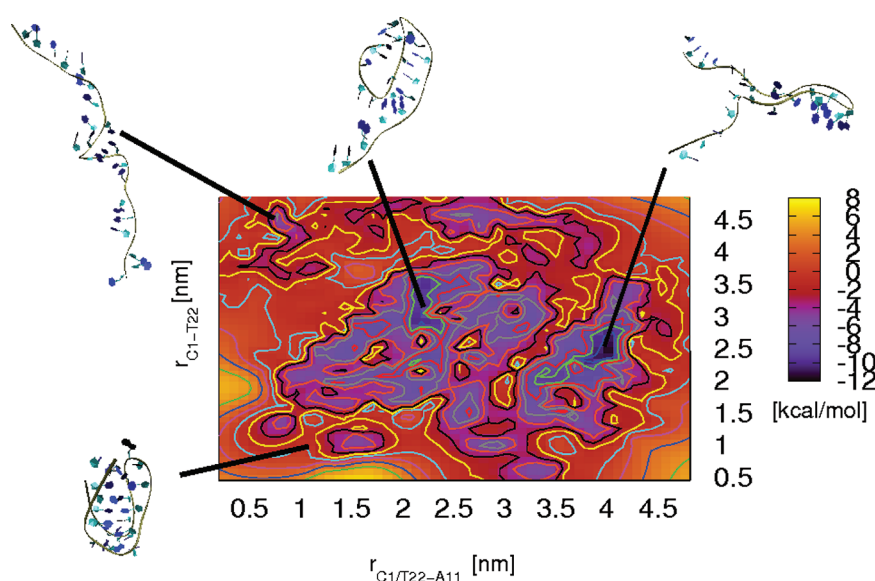


**Figure 3.** Free energy landscape at 300 K for the distances between the centers of mass for C1 and T22 to A11  $r_{C1/T22-A11}$  and the distance between C1 and T22  $r_{C1-T22}$ . The lines correspond to energy differences of 1.5 kcal/mol.

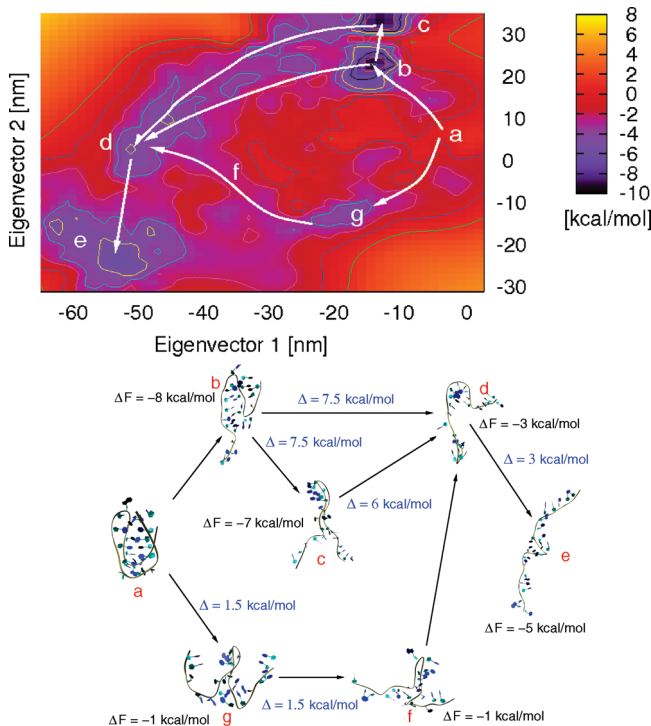


**Figure 4.** Free energy landscape for eigenvectors 1 and 2 with the corresponding stable configurations (top). The analysis of the simulation trajectory allows defining connection routes between the configurations (bottom). The configurations are characterized by their free energy differences  $\Delta F$  to the starting structure. Free energy barriers between the configurations are denoted by  $\Delta$ , whereas the notation follows the figure in the top.

conformations reveals that these structures belong to the planar and partly planar structures as shown in Figure 2 b,c. The fully unfolded strand conformation which was also observed in our biased simulations can be identified as energetically less favorable. It is worth mentioning that, after comparing the overlap of the two minima in each direction, it becomes clear that a separate calculation of the free energy for each coordinate would result in a significant decrease and error of the barriers and the minima.<sup>36</sup> Hence only the usage of a two-dimensional representation allows a faithful representation of the free energy differences.

In addition, we have calculated the free energy landscape for the essential eigenvectors of the system.<sup>30</sup> The final eigenvector energy landscape is presented in Figure 4. Two large minima denoted by “b” and “c” with free energy differences from the starting structure around  $\Delta F \approx -7$  to  $-8$  kcal/mol can be identified which belong to the hairpin structures that have been discussed above. The stretched structure “e” with a free energy difference of  $-5$  kcal/mol represents a metastable minimum. All values are in good agreement with the results shown in Figure 3. Additionally, we have analyzed the trajectories of biased and high temperature simulations,<sup>31</sup> where the results are schematically presented at the bottom of Figure 4. The routes between the conformations are illustrated by arrows. It becomes clear that the corresponding energetic barriers of  $\Delta \approx 6$ – $7.5$  kcal/mol preserve the hairpin structures from unfolding. Further metastable structures denoted by “d”, “f”, and “g” can be additionally identified which represent local minima and are dominated by twisted conformations.

The one-dimensional representation for each eigenvector is presented on the left side of Figure 5, whereas the corresponding concerted eigenvectors are illustrated on the right side. Eigenvector 1 describes the variation of the end-to-end distance by a stretching motion, whereas eigenvector 2 mainly captures the relaxation from the starting to the planar structure.

The one-dimensional landscapes again reveal the hairpin structures as stable conformations with averaged barrier heights of  $6$  kcal/mol for eigenvector 1 and  $5$  kcal/mol for eigenvector 2, in good agreement with the results shown above. Thus all our findings indicate the dominance of deprotonated hairpin structures at  $300$  K. The native starting form is energetically unfavorable in agreement with the disappearance of a deprotonated i-motif in solution.<sup>1,2</sup>

**4.3. Thermodynamic Properties at 300 K.** For a more detailed study of the stable structures, we have calculated the total energy and the temperature–entropy contribution shown in Table 1 for each configuration of Figure 4 relative to the native structure. The total entropy is given by the relation  $\Delta S = (\Delta U - \Delta F)/T$ , where  $\Delta F$  and  $\Delta U$  denote the free and the total energy differences whereas  $T$  represents the system temperature. Surprisingly, it comes out that the most favorable conformations in terms of the total energy  $\Delta U$  are represented by structures d, f, and g in contrast to the free energy landscapes shown above. Furthermore, it is evident that the energetic contributions to the free energy for these conformations are compensated by the deficit of entropic energy as can be seen by the large negative values for  $T\Delta S$ .

It is remarkable that all structures compared to the unstable starting configuration are entropically less favorable. This can be related to an enhanced ordering of water molecules as we will show in the following.

To prove this point, we have studied the entropic contributions  $\Delta S = \Delta S_e + \Delta S_c$  for each structure individually, where  $\Delta S_e$  represents the change in the environmental entropy and  $\Delta S_c$  is the change of the configurational entropy as calculated by a quasi-harmonic approach.<sup>37</sup> The results are shown in Table 2. All structures are comparable in their configurational entropy gain as can be seen by the nearly identical values for  $\Delta S_c$ . Hence it is obvious that the most significant contribution to the total entropy must arise from the change in the environmental entropy,  $\Delta S_e$ . It is obvious that the largest deficits for  $\Delta S_e$  occur for structures d, f, and g, which indicates them as less preferable in agreement with the free energy differences shown in Table 1.

An explanation for the strong variation of  $\Delta S_e$  for each structure and the total energy difference  $\Delta U$  presented in Table 1 can be given by the number of solvent hydrogen bonds  $\Delta n_H$  relative to the starting structure (Table 2). It is evident that increased values for the number of hydrogen bonds lead to lower total energies  $\Delta U$  (Table 1). In combination it can be also seen that the values for the entropy differences significantly decrease. The hairpin structures b and c are therefore entropically more preferable due to smaller values for  $\Delta n_H$ . The total energy gain of all other structures is compensated by the large deficits of the entropic energy contributions. This behavior can be also directly understood by a visual analysis of the conformations shown in Figures 2 and 4. The small increase of  $\Delta n_H$  for structures b and c becomes clear by noticing the fact that most of the nucleobases are not directly accessible to water molecules. To prove this point, we have calculated the solvent accessible hydrophilic surface area.<sup>38</sup> An increase of the area compared to the starting structure is given by  $7.24 \text{ nm}^2$  for b,  $4.31 \text{ nm}^2$  for c,  $6.94 \text{ nm}^2$  for d,

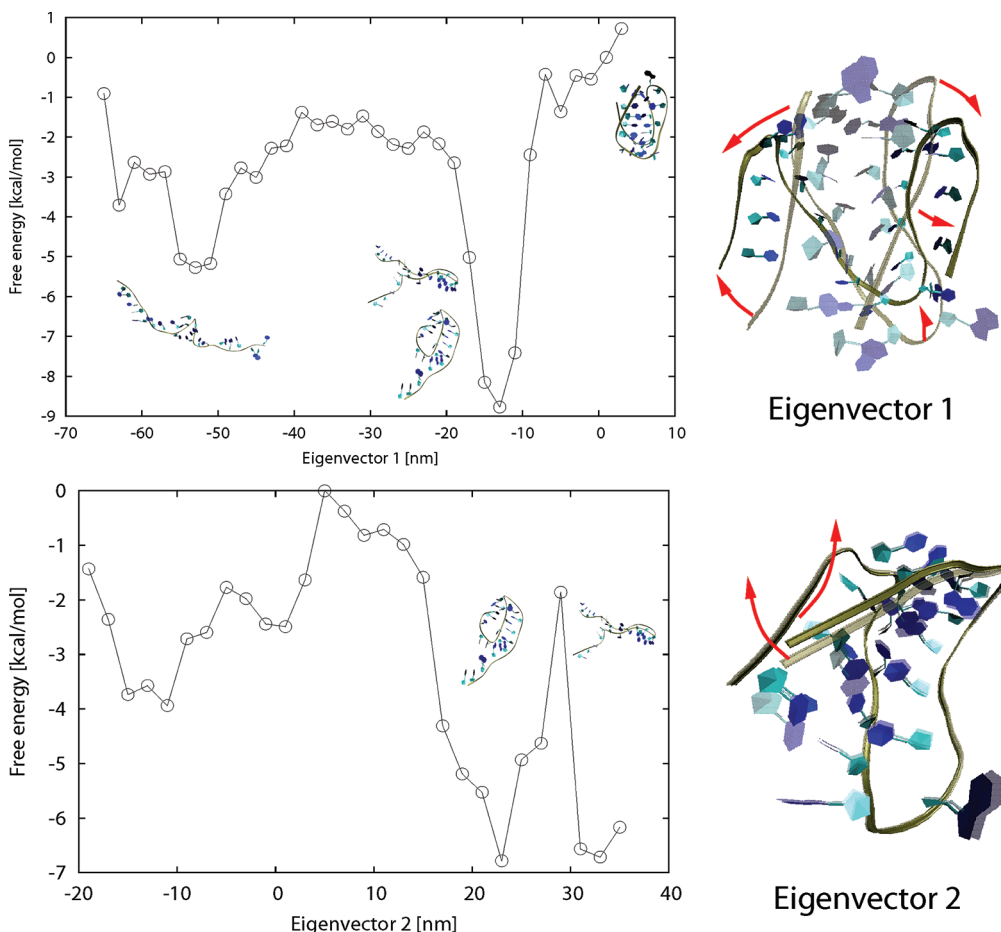


**Figure 5.** Free energy landscape for the one-dimensional representation along eigenvector 1 (top left) and eigenvector 2 (bottom left) with the corresponding conformations. The values for eigenvector 2 have been computed along the values  $-20$  to  $-10$  nm of eigenvector 1. The concerted motion of eigenvectors 1 and 2 is shown in the right as indicated by the red arrows.

**Table 1. Total Energy  $\Delta U$  and Temperature–Entropy Contribution  $T\Delta S$  to the Free Energy Difference  $\Delta F$  for the Different Configurations Shown in Figure 4 Relative to the i-Motif Structure**

configuration	$\Delta U$ [kcal/mol]	$T\Delta S$ [kcal/mol]	$\Delta F$ [kcal/mol]
b	-59	-51	-8
c	-21	-14	-7
d	-127	-124	-3
e	-62	-57	-5
f	-140	-139	-1
g	-177	-176	-1

$11.31 \text{ nm}^2$  for e,  $5.94 \text{ nm}^2$  for f, and finally  $6.95 \text{ nm}^2$  for g. Hence it becomes clear that a larger hydrophilic surface area leads to a larger number of hydrogen bonds such that the environmental entropy is lowered. Thus it is reasonable to assume that the occurrence of hairpin structures as stable conformations can be mainly explained by entropic preference due to a lower ordering of the local solvent shell.

**4.4. Thermodynamic Properties at 500 K.** We have also calculated the thermodynamic properties at 500 K. The presented results have been achieved by high temperature simulations in which we have identified a fully unfolded strand as the

**Table 2. Total Entropy  $\Delta S$ , Configurational Entropy  $\Delta S_c$ , Environmental Entropy  $\Delta S_e$ , and Number of Solvent Hydrogen Bonds  $\Delta n_H$  for the Different Configurations Shown in Figure 4 Relative to the i-Motif Structure**

configuration	$\Delta S$ [kcal/K mol]	$\Delta S_c$ [kcal/K mol]	$\Delta S_e$ [kcal/K mol]	$\Delta n_H$
b	-0.17	0.35	-0.52	11
c	-0.05	0.34	-0.39	1
d	-0.41	0.34	-0.75	20
e	-0.19	0.35	-0.54	31
f	-0.46	0.34	-0.80	25
g	-0.59	0.33	-0.92	37

most dominant configuration.<sup>31</sup> The shift of the equilibrium conformation can be explained by detailed analysis of the thermodynamic properties analogously to the previous section. The values for the total energy, the free energy differences as derived by the results presented in ref 31, and the temperature–entropy configuration at 500 K are shown in Table 3.

It can be seen that free energy minima are given for structures c, d, and e with  $\Delta F \approx -3 \text{ kcal/mol}$ . By regarding the values for each structure, it is obvious that the energetic differences of  $\Delta F$  are smaller compared to Table 1. This is in agreement with the

**Table 3.** Total Energy  $\Delta U$  and Temperature–Entropy Contribution  $T\Delta S$  to the Free Energy Difference  $\Delta F$  for the Different Configurations Shown in Figure 4 Relative to the i-Motif Structure at 500 K

configuration	$\Delta U$ [kcal/mol]	$T\Delta S$ [kcal/mol]	$\Delta F$ [kcal/mol]
b	-31	-29	-2
c	-7	-4	-3
d	-48	-45	-3
e	-10	-7	-3
f	-47	-45	-2
g	-108	-106	-2

**Table 4.** Total Entropy  $\Delta S$ , Configurational Entropy  $\Delta S_c$ , Environmental Entropy  $\Delta S_e$ , and Number of Hydrogen Bonds  $\Delta n_H$  for the Different Configurations Shown in Figure 4 Relative to the i-Motif Structure at 500 K

configuration	$\Delta S$ [kcal/K mol]	$\Delta S_c$ [kcal/K mol]	$\Delta S_e$ [kcal/K mol]	$\Delta n_H$
b	-0.05	0.44	-0.49	11
c	-0.01	0.43	-0.44	1
d	-0.09	0.44	-0.53	20
e	-0.01	0.45	-0.46	23
f	-0.09	0.43	-0.52	17
g	-0.21	0.43	-0.61	26

smaller number of hydrogen bonds (Table 4) and with the smaller decrease of  $\Delta U$  and  $T\Delta S$  compared to the results obtained at 300 K. Regarding the increased values for the configurational entropy difference  $\Delta S_c$  as shown in Table 4, it is clear that a main reason for this behavior is given by thermal activation of additional degrees of freedom at higher temperatures. It is also evident that the values for  $\Delta S_e$  are more weakly dependent on  $\Delta n_H$  than at lower temperatures. In addition, a general decrease of  $\Delta n_H$  can be observed for structures e–g as presented in Table 4. Hence it can be concluded that the effects of water ordering are less pronounced at higher temperatures due to a smaller number of solvent hydrogen bonds. Combining the results, it comes out that the weaker ordering of the solvent shell at 500 K leads to smaller variations of the entropic contributions as well as for the total energy. This finally results in temperature dependent free energy minima such that the presence of the hairpin structures at 300 K is shifted to a fully unfolded conformation at 500 K.

**4.5. Hydrogen Bonds.** To study the properties of  $\Delta n_H$  for different configurations in more detail, we have calculated the ratio of solvent hydrogen bonds for backbone and nonbackbone atoms compared to the starting structure. The results for 300 K are presented in Figure 6. It is obvious that the backbone ratio is nearly constant for each structure. A significant increase of nonbackbone hydrogen bonds coming from nucleobase–water interactions can be observed for all conformations except c. This is in good agreement with the results for the increase of the solvent accessible hydrophilic surface area as reported in section 4.3. It can be assumed that the solvent hydrogen bonds with the nonbackbone atoms are energetically less stable due to smaller partial charge values. This is obvious by regarding the lifetimes for backbone hydrogen bonds  $\tau_{bb}$  and nonbackbone atoms  $\tau_{nb}$

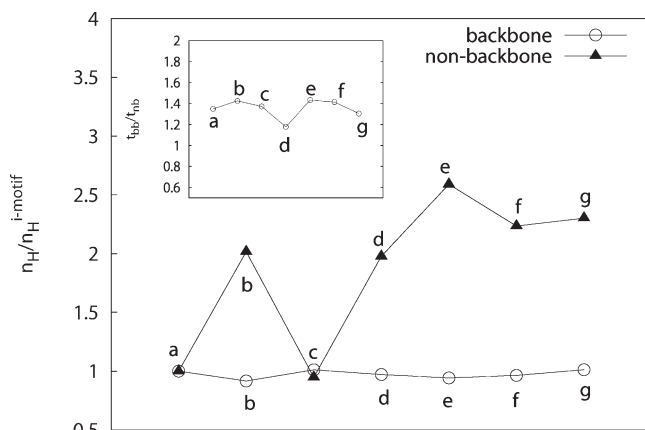


**Figure 6.** Ratio of backbone and nonbackbone hydrogen bonds  $n_H$  compared to the i-motif  $n_H^{i\text{-motif}}$  for each configuration at 300 K. Inset: Ratio of the lifetimes for backbone hydrogen bonds  $\tau_{bb}$  and nonbackbone hydrogen bonds  $\tau_{nb}$  for each configuration at 300 K. The lines are only for the eyes.

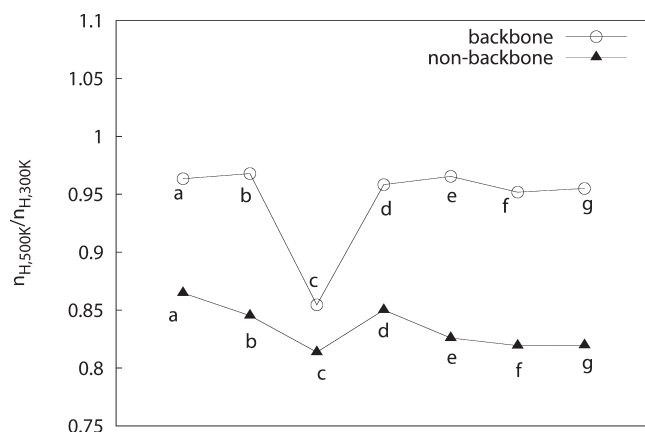


**Figure 7.** Ratio of the number of hydrogen bonds  $n_{H,500\text{ K}}/n_{H,300\text{ K}}$  at 500 and 300 K for nonbackbone and backbone atoms. The lines are only for the eyes.

shown in the inset of Figure 6. It comes out that  $\tau_{bb}/\tau_{nb} > 1$  for all structures.

The properties of the hydrogen bonds at 500 K compared to the hydrogen bonds at 300 K are presented in Figure 7, where the ratio  $n_{H,500\text{ K}}/n_{H,300\text{ K}}$  is shown. In agreement with the discussion above, it is obvious that backbone hydrogen bonds are energetically more stable than nonbackbone hydrogen bonds as becomes evident by the presented larger ratios. Thus we have validated that the decrease of  $\Delta n_H$  observed at 500 K is mainly induced by a smaller number of nonbackbone hydrogen bonds compared to 300 K.

**4.6. Experimental Results.** The stability of the hairpin structures at 300 K and the appearance of the unfolded structures at higher temperatures is also supported by regarding the results of circular dichroism (CD) spectropolarimetry. CD spectra of i-motifs at two different temperatures, 298.15 and 368.15 K, and at pH 8 are presented in Figure 8. The deprotonated i-motif structure is in general validated by negative CD minima at 297 nm.<sup>39</sup> It has been reported in refs 40 and 41 that the hemiprotonated DNA i-motif has a maximum at 285 nm, a negative

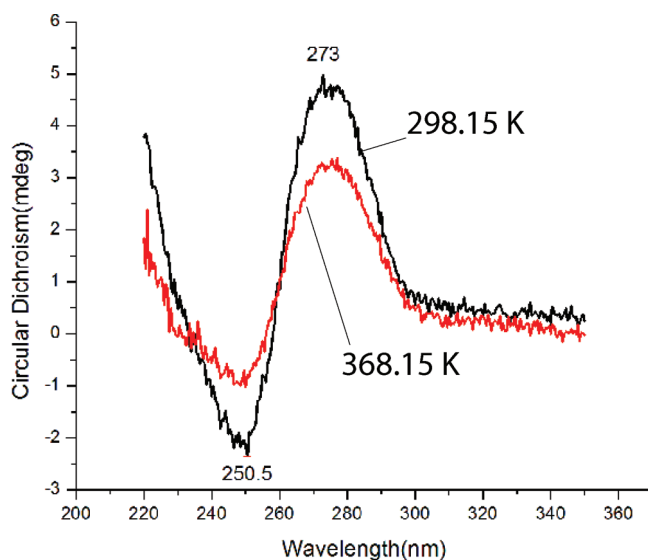


**Figure 8.** CD spectra at 298.15 (black) and 368.15 K (red) of a deprotonated DNA i-motif in basic solution. The small numbers denote the positions of the minima and maxima.

minimum at 260 nm, and a crossover at 270 nm. Hence the results shown in Figure 8 display an absence of the i-motif which is indicated by a shifted maximum at 273 nm, a minimum at 250.5 nm, and a crossover at 257 nm. It must be noticed that at pH 7.2 similar CD spectra have been derived<sup>18</sup> which validate the presence of stable hairpin structures.

In general, it was discussed in refs 42 and 43 that the intensity of the minima is given by the number of connected base pairs and intramolecular interaction energies. Hence it can be seen in Figure 8 that the smaller values for 368.15 K indicate a decrease of intramolecular interactions. This is in agreement with the numerical results which have validated the presence of a fully unfolded strand at higher temperatures where intramolecular interactions are mainly absent as can be also seen by the distance matrices shown in Figure 2. Hence we conclude that the experimental results are in good agreement with our numerical findings. We have experimentally validated that the hairpin structures are representing the global minima at lower temperatures while a fully unfolded configuration can be found at increased temperatures.

## 5. SUMMARY AND CONCLUSION

We have studied the stable structures of a deprotonated DNA i-motif via molecular dynamics simulations in explicit solvent. Our results indicate hairpin structures as the most stable configurations in the absence of protonated cytosines. This validates that the deprotonated i-motif is not stable at room temperature in agreement with earlier published experimental results.<sup>2,6,18</sup> By a study of the thermodynamic properties, we have found that the reason for this behavior is mainly given by entropic preferences due to the present number of hydrogen bonds. The nature of these bonds and their importance for a temperature dependent entropy have been investigated in detail. We have also identified large energy barriers between each configuration which prevent the equilibrium structures from unfolding.

In addition, it has been found that at 500 K the global minimum configuration is given by a fully unfolded strand. This behavior

can be explained by a lower number of solvent hydrogen bonds such that the surrounding water shell is less ordered compared to 300 K. We conclude that the presence of the free energy minima is mainly determined by a combination of the environmental entropy and the total energy.

The presented numerical results are in good agreement with experimental CD spectra. The experiments validate the presence of hairpin structures at 300 K and their absence at higher temperatures. As discussed above, we have shown that a full unfolding into a stretched structure can be observed at higher temperatures.

This sheds new light on the importance of the deprotonated structures due to the fact that often fully unfolded configurations have been discussed as global equilibrium conformations at room temperature.<sup>4,19</sup> Although it can be concluded that the presence of a large number of grafted i-motifs may lead to a significant impact on the hairpin structures, our results are a first step toward the improvement of nanocontainer fabrication for low grafting densities and the study of stable conformations at basic pH values.<sup>10</sup>

## ■ AUTHOR INFORMATION

### Corresponding Author

\*E-mail: jens.smiatek@uni-muenster.de (J.S.); andheuer@uni-muenster.de (A.H.).

## ■ ACKNOWLEDGMENT

We thank the Deutsche Forschungsgemeinschaft (DFG) through the transregional collaborative research center TRR 61 for financial funding.

## ■ REFERENCES

- (1) Gehring, K.; Leroy, J.-L.; Gueron, M. *Nature* **1993**, *363*, 561–565.
- (2) Gueron, M.; Leroy, J.-L. *Curr. Opin. Struct. Biol.* **2000**, *10*, 326–331.
- (3) Lane, A. N.; Chaires, J. B.; Gray, R. D.; Trent, J. O. *Nucleic Acids Res.* **2008**, *36*, 5482–5515.
- (4) Liu, H.; Liu, D. *Chem. Commun.* **2009**, *19*, 2625–2636.
- (5) Phan, A. T.; Mergny, J.-L. *Nucleic Acids Res.* **2002**, *30*, 4618–4625.
- (6) Zhao, Y.; Zeng, Y.-X.; Kan, Z.-Y.; Hao, Y.-H.; Tan, Z. *ChemBioChem* **2005**, *6*, 1957–1960.
- (7) Catasti, P.; Chen, X.; Deaven, L. L.; Moyzis, R. K.; Bradbury, E. M.; Gupta, G. *J. Mol. Biol.* **1997**, *272*, 369–382.
- (8) Hurley, L. H. *Biochem. Soc. Trans.* **2001**, *29*, 692–696.
- (9) Liu, D.; Balasubramian, S. *Angew. Chem.* **2003**, *42*, 5734–5736.
- (10) Mao, Y.; Liu, D.; Wang, S.; Luo, S.; Wang, W.; Yang, Y.; Ouyang, Q.; Jiang, L. *Nucleic Acids Res.* **2007**, *35*, e33.
- (11) Modi, S.; Swetha, M. G.; Goswami, D.; Gupta, G. D.; Mayor, S.; Krishnan, Y. *Nat. Nanotechnol.* **2009**, *4*, 325–330.
- (12) Pu, F.; Wang, C. Y.; Hu, D.; Huang, Z. Z.; Ren, J. S.; Wang, S.; Qu, X. G. *Mol. Biosyst.* **2010**, *6*, 1928–1932.
- (13) Peng, Y. H.; Wang, X. H.; Xiao, Y.; Feng, L. Y.; Zhao, C.; Ren, J. S.; Qu, X. G. *J. Am. Chem. Soc.* **2009**, *131*, 13813–13818.
- (14) Spackova, N.; Berger, I.; Egli, M.; Sponer, J. *J. Am. Chem. Soc.* **1998**, *120*, 6147–6151.
- (15) Gallego, J.; Golden, E. B.; Stanley, D. E.; Reid, B. R. *J. Mol. Biol.* **1999**, *285*, 1039–1052.
- (16) Malliavin, T. E.; Snoussi, K.; Leroy, J.-L. *Magn. Reson. Chem.* **2003**, *41*, 18–25.
- (17) Ahmed, S.; Henderson, E. *Nucleic Acids Res.* **1992**, *20*, 507–511.
- (18) Pataskar, S.; Dash, D.; Brahmachari, S. K. *J. Biomol. Struct. Dyn.* **2001**, *19*, 293–306.
- (19) Xia, H.; Hou, Y.; Ngai, Y.; Zhang, G. *J. Phys. Chem. B* **2010**, *114*, 775–779.

- (20) Hess, B.; Kutzner, C.; van der Spoel, D.; Lindahl, E. *J. Chem. Theory Comput.* **2008**, *4*, 435–447.
- (21) Sorin, E. J. ffAMBER—AMBER force field ports for the GROMACS molecular dynamics suite. <http://ffamber.cnsm.csulb.edu/> (accessed Oct 4, 2011).
- (22) Sorin, E. J.; Pande, V. S. *Biophys. J.* **2005**, *88*, 2472–2493.
- (23) Duan, Y.; Wu, C.; Chowdhury, S.; Lee, M. C.; Xiong, G.; Zhang, W.; Yang, R.; Cieplak, P.; Luo, R.; Lee, T.; Caldwell, J.; Wang, J.; Kollman, P. A. *J. Comput. Chem.* **2003**, *24*, 1999–2012.
- (24) Wang, J.; Cieplak, P.; Kollman, P. A. *J. Comput. Chem.* **2000**, *21*, 1049–1074.
- (25) Phan, T. A.; Gueron, M.; Leroy, J.-L. *J. Mol. Biol.* **2000**, *299*, 123–144.
- (26) Laio, A.; Parrinello, M. *Proc. Natl. Acad. Sci. U.S.A.* **2002**, *99*, 12562–12566.
- (27) Bonomi, M.; Branduardi, D.; Bussi, G.; Camilloni, C.; Provasi, D.; Raiteri, P.; Donadio, D.; Marinelli, F.; Pietrucci, F.; Broglia, R. A.; Parrinello, M. *Comput. Phys. Commun.* **2009**, *180*, 1961–1972.
- (28) Kumar, S.; Rosenberg, J. M.; Bouzida, D.; Swenden, R.; Kollman, P. A. *J. Comput. Chem.* **1992**, *13*, 1011–1021.
- (29) Smiatek, J.; Heuer, A. *J. Comput. Chem.* **2011**, *32*, 2084–2096.
- (30) Amadei, A.; Linsen, A. B. M.; Berendsen, H. J. C. *Proteins* **1993**, *17*, 412–425.
- (31) Smiatek, J.; Liu, D.; Heuer, A. *Curr. Phys. Chem.* **2011**.
- (32) Laio, A.; Gervasio, F. L. *Rep. Prog. Phys.* **2008**, *71*, 126601–126623.
- (33) Ensing, B.; de Vivo, M.; Liu, Z.; Moore, P.; Klein, M. L. *Acc. Chem. Res.* **2005**, *39*, 73–81.
- (34) Ensing, B.; Laio, A.; Parrinello, M.; Klein, M. L. *J. Phys. Chem. B* **2005**, *109*, 6676–6687.
- (35) Dobson, C. M.; Sali, A.; Karplus, M. *Angew. Chem., Int. Ed.* **1998**, *37*, 868–893.
- (36) Bolhuis, P. G.; Dellago, C.; Geissler, P. L.; Chandler, D. *Annu. Rev. Phys. Chem.* **2002**, *54*, 291–318.
- (37) Andricioaei, I.; Karplus, M. *J. Chem. Phys.* **2001**, *115*, 6289–6292.
- (38) Eisenhaber, F.; Lijnzaad, P.; Argos, P.; Sander, C.; Scharf, M. *J. Comput. Chem.* **1995**, *16*, 273–284.
- (39) Mathur, V.; Verma, A.; Maiti, S.; Chowdhury, S. *Biochem. Biophys. Res. Commun.* **2004**, *320*, 1220–1227.
- (40) Pataskar, S. S.; Dash, D.; Brahmachari, S. K. *J. Biomol. Struct. Dyn.* **2001**, *19*, 307–313.
- (41) Xu, Y.; Sugiyama, H. *Nucleic Acids Res.* **2006**, *34*, 949–954.
- (42) Rentzepis, D.; Shikiya, R.; Maiti, S.; Ho, J.; Marky, L. A. *J. Phys. Chem. B* **2002**, *106*, 9945–9950.
- (43) Tuma, J.; Tonzani, S.; Schatz, G. C.; Karaba, A. H.; Lewis, F. D. *J. Phys. Chem. B* **2007**, *111*, 13101–13106.